IRIS AperTO

UNIVERSITÀ DEGLI STUDI DI TORINO

AperTO - Archivio Istituzionale Open Access dell'Università di Torino

Piezo-optic and elasto-optic properties of monoclinic triglycine sulfate crystals

This is the author's manuscript

Original Citation:

Availability:

This version is available http://hdl.handle.net/2318/1667189 since 2018-04-30T15:28:35Z

Terms of use:

Open Access

Anyone can freely access the full text of works made available as "Open Access". Works made available under a Creative Commons license can be used according to the terms and conditions of said license. Use of all other works requires consent of the right holder (author or publisher) if not exempted from copyright protection by the applicable law.

(Article begins on next page)

06 May 2024

Piezooptic and elastooptic properties of monoclinic triglycine sulfate crystals

Bogdan Mytsyk [1], Natalya Demyanyshyn [1], Alessandro Erba [2], Viktor Shut [3], Sergey Mozzharov [3], Yaroslav Kost [1], Oksana Mys [4] and Rostyslav Vlokh * [4]

[1] N. V. Karpenko Physico-Mechanical Institute, 5 Naukova Street, 79601 Lviv, Ukraine

[2] Universita di Torino, Via Giuria 5, 10125 Torino, Italy

[3] Institute of Technical Acoustics of NAS of Belarus, 13 Lyudnykov Avenue, 220023 Vitebsk, Belarus

[4] Vlokh Institute of Physical Optics, 23 Dragomanov Street, 79005 Lviv, Ukraine

Abstract. For the first time we have experimentally determined all of the components of piezooptic tensor for monoclinic crystals. This has been implemented on a specific example of TGS crystals. Basing on the results obtained, the complete elastooptic tensor has been calculated. The acoustooptic figures of merit (AOFM) have been estimated for the case of acoustooptic interaction occurring in the principal planes of optical indicatrix ellipsoid and for the geometries in which the highest elastooptic coefficients are involved as effective parameters. It has been found that the highest AOFM value is equal to 6.8×10^{-15} s^3/kg for the case of isotropic acoustooptic interaction with quasi-longitudinal acoustic waves in the principal planes. This AOFM is higher than the corresponding values typical for the canonic acoustooptic materials, which are transparent in the deep ultraviolet spectral range.

Keywords: monoclinic crystals, piezooptic coefficients, elastooptic coefficients, acoustooptic materials, acoustooptic figures of merit.

1. Introduction

Piezooptic effect consists in changes of refractive indices n of a material medium under the action of mechanical stresses σ_m. It represents a well-known phenomenon discovered by David Brewster as early as in 1816 [1]. A similar effect, which is often called as elastooptic, is described in terms of the mechanical strains e_n (see, e.g., Ref. [2]). The both effects can be represented using the relations

$$\Delta B_i = B_i^0 - B_i = \pi_{im}\sigma_m = p_{in}e_n, \quad p_{in} = \pi_{im}C_{mn}, \tag{1}$$

where π_{im} and p_{il} are respectively the piezooptic and elastooptic tensors, $B_i^0 = \left(1/n^2\right)_i$ and B_i the optical-frequency impermeability tensors defined under the conditions of absence and presence of mechanical stresses (or strains), and C_{mn} is the tensor of elastic-stiffness coefficients.

The piezooptic and elastooptic effects have found their applications in different optical and optoelectronic devices, e.g. for determining mechanical stresses, including a so-called stress-tensor field tomography, in remote stress sensors, accelerometers and light-polarization modulators (see Refs. [2–7]).

One of the most important applications of the elastooptic effect is concerned with acoustooptic devices [8–10]. When searching for efficient geometries of acoustooptic interactions, one has to know both the magnitudes and signs of all of the elastooptic tensor components [11–15]. In this respect it is noteworthy that the most precise and widely used acoustooptic Dixon–Kohen method for measuring the elastooptic coefficients does not enable determining their signs [16, 17]. Only interferometric and polarimetric methods are fit for measuring the piezooptic tensor coefficients and recalculating them into the elastooptic components [18–22]. This can be complied using Eqs. (1) and elastic stiffness coefficients known in advance. However, one has to keep in mind that the recalculation procedure itself increases the appropriate errors notably.

When the symmetry of crystals becomes lower, the numbers of independent components of all the tensors increase. This complicates further the problems with the errors. For instance, even for orthorhombic SrB_4O_7 crystals, for which the piezooptic and elastooptic matrices contain twelve independent components, some of the piezooptic tensor components have been determined, using the interferometric technique with the error exceeding 50%, while the calculation errors for some of the elastooptic coefficients have already been as high as 100% [23]. Such errors can make no sense of further determining preferable acoustooptic geometries. In our recent works [24, 25] we have shown that the piezooptic errors resulting from the methods based upon uniaxial loading of samples originate from barrel-like strains appearing in parallelepiped-shaped samples. They arise due to friction forces acting among the sample bulk and its top and bottom substrates. In its turn, this brings about inhomogeneous stresses inside samples, of which spatial distribution is unknown. To avoid such inhomogeneous stresses, we have developed a number of methods for measuring the piezooptic coefficients, which are based on applying torsion or bending stresses to samples. Although these stresses are also non-uniform, their distribution can be known in advance [26–28]. On the other hand, these methods reveal a shortcoming associated with significant number of samples with special orientations and sizes, which are needed experimentally. Moreover, this number increases drastically with lowering crystalline symmetry. As a consequence, traditional interferometric techniques based on uniaxial loading of samples become indispensable in the latter case.

Issuing from the arguments mentioned above, one can see that the problems with accurate measurements of the piezooptic coefficients are the most prominent if one studies low-symmetry crystals. In the present work we will demonstrate that the interferometric method accompanied by uniaxial loading of samples can, in principle, be used for determining the piezooptic coefficients of monoclinic crystals. This will be done on a specific example of triglycine sulfate (TGS) crystals. As a result, a full matrix of the piezooptic coefficients of monoclinic crystals will be obtained for the first time.

2. Relations for the piezooptic coefficients and experimental procedures

TGS crystals described by the chemical formula $(NH_2CH_2COOH)_3H_2SO_4$ represent a canonical ferroelectric material belonging to the point symmetry groups 2 and 2/m respectively below and above the Curie temperature (T_C = 322 K) [29]. The matrix of piezooptic (or elastooptic) tensor for all monoclinic groups is the same and contains twenty independent components [30]. In our recent work [31] we have deter-

mined the nine 'principal' components π_{im} given by the indices *i*, *m* = 1, 2 and 3. The remaining eleven unknown components are π_{15}, π_{25}, π_{35}, π_{51}, π_{52}, π_{53}, π_{44}, π_{55}, π_{66}, π_{46} and π_{64}. These 'non-principal' coefficients are harder to be determined, since the corresponding theoretical relations usually include a complicated combination of different piezooptic components and elastic compliances [32]. In fact, this is the reason of the high errors arising in case if one determines these coefficients. In this work we have derived simplified relations for determining the non-principal piezooptic coefficients, following from so-called 'symmetric' experimental conditions.

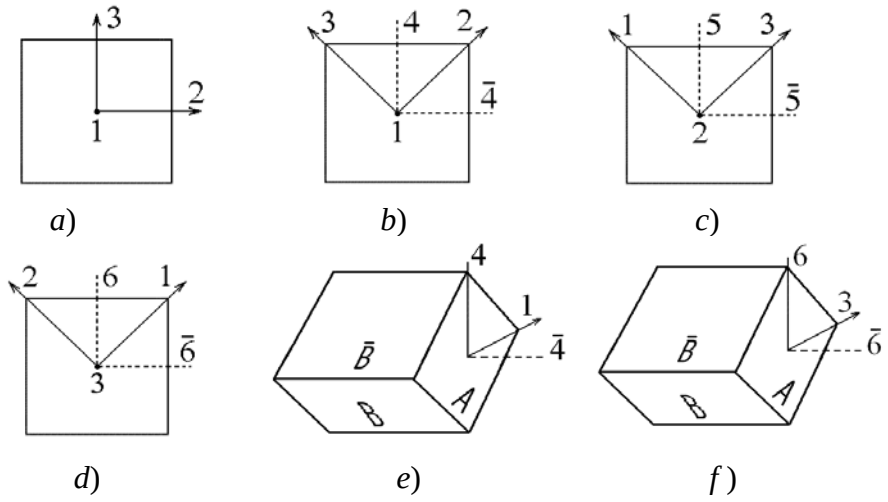

Fig. 1. Schematic presentation of samples used for studying the piezooptic effect in crystals: (a) one of direct cuts, (b) *X*/45°-cut, (c) *Y*/45°-cut, (d) *Z*/45°-cut, (e) *B* and $\bar{4}$-cuts, and (f) *B* and $\bar{6}$-cuts.

Below we consider the symmetric experimental conditions, which are described by the indices 4 and $\bar{4}$, 5 and $\bar{5}$, 6 and $\bar{6}$, as well as *B* and $\bar{B}$. Let a standard method of half-wave stresses be used. Then the relation for the piezooptic coefficient π_{46} under the experimental conditions $i = 4$, $k = \bar{4}$ and $m \perp B$ are written as [32]

$$\pi_{22} + \pi_{23} + \pi_{32} + \pi_{33} + 2(\pi_{21} + \pi_{31} + \pi_{44}) + \sqrt{2}(\pi_{25} + \pi_{35} + \pi_{46}) = -\frac{8\lambda}{n_4^3 \sigma_{4B}^{\circ}} \qquad (2)$$
$$+2\frac{S_{22} + S_{33} - S_{44} + 2(S_{12} + S_{13} + S_{23}) + \sqrt{2}(S_{25} + S_{35} - S_{46})}{n_4^3}(n_4 - 1),$$

where S_{km} denote the elastic-compliance coefficients, the indices *i*, *k* and *m* indicate respectively the directions of light polarization, light propagation and uniaxial load, $\sigma_{4B}^{\circ} = \sigma_{4B} d_{\bar{4}}$ is the control stress, σ_{4B} the half-wave stress, $d_{\bar{4}}$ the sample thickness along the light propagation direction (see Fig. 1e), and λ = 632.8 nm the wavelength of optical radiation. The directions indicated by the indices 1, 2 and 3 correspond respectively to the principal axes of optical indicatrix (–*X*), *Y* and *Z*, whereas the directions given by the indices 4, 5 and 6 correspond to the bisectors *YZ*, *XZ* and *XY*, respectively. Then the directions indicated respectively as $\bar{4}$, $\bar{5}$ and $\bar{6}$ represent the bisectors *Y*(–*Z*) [or (–*Y*)*Z*], *Z*(–*X*) [or (–*Z*)*X*] and *X*(–*Y*) [or (–*X*)*Y*] (see Fig. 1).

The refractive indices for the light polarized along these bisector directions read as

$$n_4 = \frac{\sqrt{2}}{\sqrt{B_2 + B_3}} = \frac{\sqrt{2}n_2 n_3}{\sqrt{n_2^2 + n_3^2}},\ n_5 = \frac{\sqrt{2}}{\sqrt{B_1 + B_3}} = \frac{\sqrt{2}n_1 n_3}{\sqrt{n_1^2 + n_3^2}},\ n_6 = \frac{\sqrt{2}}{\sqrt{B_1 + B_2}} = \frac{\sqrt{2}n_1 n_2}{\sqrt{n_1^2 + n_2^2}}, \tag{3}$$

where $B_1 = 1/n_1^2,\ B_2 = 1/n_2^2, B_3 = 1/n_3^2$ are the diagonal impermeability tensor components, and n_1, n_2 and n_3 the principal refractive indices. The relation corresponding to the symmetric experimental conditions (i.e., to the direction of uniaxial loading $m \perp \bar{B}$) is given by

$$\begin{aligned} &\pi_{22} + \pi_{23} + \pi_{32} + \pi_{33} + 2(\pi_{21} + \pi_{31} + \pi_{44}) - \sqrt{2}(\pi_{25} + \pi_{35} + \pi_{46}) = -\frac{8\lambda}{n_4^3 \sigma_{4B}^{\circ}} \\ &+2\frac{S_{22} + S_{33} - S_{44} + 2(S_{12} + S_{13} + S_{23}) - \sqrt{2}(S_{25} + S_{35} - S_{46})}{n_4^3}(n_4 - 1)\,. \end{aligned} \tag{4}$$

Subtracting Eqs. (2) and (4), one obtains

$$\pi_{25} + \pi_{35} + 2\pi_{46} = -\frac{2\sqrt{2}\,\lambda}{n_4^3} + \left(\frac{1}{\sigma_{4B}^{\circ}} - \frac{1}{\sigma_{4\bar{B}}^{\circ}}\right) + 2\frac{S_{25} + S_{35} - S_{46}}{n_4^3}(n_4 - 1), \tag{5}$$

on the basis of which one can determine the coefficient π_{46}, whenever the π_{25} and π_{35} coefficients are known.

Similar relations can be obtained for all of the eleven piezooptic components, as seen from Table 1. Notice also that some of the relations presented in Table 1 contain the principal piezooptic coefficients. This fact can be used for verifying the values of the coefficients obtained with the samples of so-called direct cuts.

Table 1. Theoretical relations used for determining non-principal piezooptic coefficients of monoclinic crystals.

Experimental conditions	Relation
	Sample of *X*/45°-cut (Fig. 1b)
m = 4($\bar{4}$) k = $\bar{4}$(4) i = 4($\bar{4}$)	$\pi_{44} = -\frac{2\lambda}{n_4^3 \sigma_{44(\bar{4}\bar{4})}^{\circ}} + (S_{22} + 2S_{23} + S_{33} - S_{44})\frac{n_4 - 1}{n_4^3} - (\pi_{22} + \pi_{23} + \pi_{32} + \pi_{33})/2$
	Sample of *Y*/45°-cut (Fig. 1c)
m = 2 k = $\bar{5}$(5) i = 5($\bar{5}$)	$\pi_{52} = -\frac{\lambda}{2n_5^3}\left(\frac{1}{\sigma_{52}^{\circ}} - \frac{1}{\sigma_{\bar{5}2}^{\circ}}\right) - S_{25}\frac{n_5 - 1}{n_5^3}$
m = 5($\bar{5}$) k = 2 i = 1	$\pi_{15} = -\frac{\lambda}{n_1^3}\left(\frac{1}{\sigma_{15}^{\circ}} - \frac{1}{\sigma_{1\bar{5}}^{\circ}}\right) + 2S_{25}\frac{n_1 - 1}{n_1^3}$
m = 5($\bar{5}$) k = 2 i = 3	$\pi_{35} = -\frac{\lambda}{n_1^3}\left(\frac{1}{\sigma_{35}^{\circ}} - \frac{1}{\sigma_{3\bar{5}}^{\circ}}\right) + 2S_{25}\frac{n_3 - 1}{n_3^3}$
m = 5($\bar{5}$) k = $\bar{5}$(5) i = 2	$\pi_{25} = -\frac{\lambda}{n_2^3}\left(\frac{1}{\sigma_{25}^{\circ}} - \frac{1}{\sigma_{2\bar{5}}^{\circ}}\right)$

$m = 5(\bar{5})$ $k = \bar{5}(5)$ $i = 5(\bar{5})$	$\pi_{55} = -\frac{\lambda}{n_5^3}\left(\frac{1}{\sigma_{55}^o} + \frac{1}{\sigma_{\bar{5}\bar{5}}^o}\right) + (S_{11} + 2S_{13} + S_{33} - S_{55})\frac{n_5 - 1}{n_5^3} - (\pi_{11} + \pi_{13} + \pi_{31} + \pi_{33})/2$
	$\pi_{51} + \pi_{53} = -\frac{\lambda}{n_5^3}\left(\frac{1}{\sigma_{55}^o} - \frac{1}{\sigma_{\bar{5}\bar{5}}^o}\right) - (\pi_{15} + \pi_{35})/2$
	Sample of *Z*/45°-cut (Fig. 1d)
$m = 6(\bar{6})$ $k = \bar{6}(6)$ $i = 6(\bar{6})$	$\pi_{66} = -\frac{\lambda}{n_6^3 \sigma_{66(\bar{6}\bar{6})}^o} + (S_{11} + 2S_{12} + S_{22} - S_{66})\frac{n_6 - 1}{n_6^3} - (\pi_{11} + \pi_{12} + \pi_{21} + \pi_{22})/2$
	Sample of *B* and $\bar{4}$-cuts (Fig. 1e)
$m \perp B(\bar{B})$ $k = \bar{4}$ $i = 4$	$\pi_{46} = -\frac{\sqrt{2}\,\lambda}{n_4^3} + \left(\frac{1}{\sigma_{4B}^o} - \frac{1}{\sigma_{4\bar{B}}^o}\right) + (S_{25} + S_{35} - S_{46})\frac{n_4 - 1}{n_4^3} - (\pi_{25} + \pi_{35})/2$
	Sample of *B* and $\bar{6}$-cuts (Fig. 1f)
$m \perp B(\bar{B})$ $k = \bar{6}$ $i = 6$	$\pi_{64} = -\frac{\sqrt{2}\,\lambda}{n_6^3} + \left(\frac{1}{\sigma_{6B}^o} - \frac{1}{\sigma_{6\bar{B}}^o}\right) + (S_{15} + S_{25} - S_{46})\frac{n_6 - 1}{n_6^3} - (\pi_{15} + \pi_{25})/2$

We have determined the absolute values of the piezooptic coefficients using a Mach–Zehnder interferometer. This can be done through measuring the half-wave mechanical stresses. According to the definition, application of these stresses leads to the difference of optical paths between the objective and reference arms of interferometer, which is equal to the half of optical wavelength. The measuring method has been described in detail in our recent work [31].

Our single crystals have been grown from aqueous solution at the Institute of Technical Acoustics of NAS of Belarus, with the average sizes of parallelepiped-shaped samples being equal to $7 \times 7 \times 7$ mm^3. The piezooptic coefficients have been measured in the coordinate system *XYZ*. The axes of this system coincide with the principal axes of the optical indicatrix ellipsoid. Note that the crystallographic coordinate system *abc* for the monoclinic TGS crystals is not rectangular. The monoclinic angle is large enough, ~ 105 deg [33]. The axes defined crystallographically are the *b* (i.e., *Y*) and *c*. We form a working Cartesian coordinate system $X_1X_2X_3$ basing on the crystallographic system, so that the axes *b* and *c* are parallel respectively to X_2 and X_3, while the axis X_1 is perpendicular to the *bc* plane.

Different constitutive coefficients of the TGS crystals, in particular the elastic-stiffness coefficients [34], are defined in the coordinate system $X_1X_2X_3$. Under normal conditions and at λ = 632.8 nm, the coordinate system *XYZ* is rotated with respect to the system $X_1X_2X_3$ by 3º around the two-fold symmetry axis (i.e., the *b* axis) [33]. The principal refractive indices at 632.8 nm are equal to $n_1 = 1.591$, $n_2 = 1.488$ and $n_3 = 1.563$ [35]. We have taken the elastic stiffnesses from Ref. [34] and rewritten their matrix in the coordinate system *XYZ* (see Table 2). Finally, the elastic compliances have been determined using the known relations $S_{mk} = (C_{mk})^{-1}$.

Table 2. Elastic-stiffness and compliance coefficients for the TGS crystals written in the coordinate systems $X_1X_2X_3$ [34] and *XYZ*.

C_{mk}, GPa	C_{11}	C_{12}	C_{13}	C_{22}	C_{23}	C_{33}	C_{15}	C_{25}	C_{35}	C_{44}	C_{55}	C_{66}	C_{46}
Coordinate system $X_1X_2X_3$	45.5	17.2	19.8	32.1	20.8	26.3	–3.0	–0.36	–5.0	9.5	11.1	6.2	–0.26
Coordinate system *XYZ*	46.1	17.2	19.9	32.1	20.7	25.3	–2.8	–0.55	–4.1	9.5	11.3	6.2	–0.43
S_{km}, 10^{-12} m^2/N	S_{11}	S_{12}	S_{13}	S_{22}	S_{23}	S_{33}	S_{15}	S_{25}	S_{35}	S_{44}	S_{55}	S_{66}	S_{46}
Coordinate system $X_1X_2X_3$	32.9	–2.9	–22.7	69.8	–57.7	108.5	–1.4	–24.5	40.9	105.4	107.3	161.5	4.4
Coordinate system *XYZ*	34.0	–0.49	–27.8	69.8	–60.1	117.5	–9.3	–21.5	44.7	106.0	102.6	160.9	7.3

As seen from Table 2, the elastic-stiffness coefficients in the both coordinate systems are almost the same. The only exceptions are the coefficients C_{46} and C_{25}. However, the components of the elastic-compliance tensor in the coordinate system *XYZ* differ significantly from those written in the coordinate system $X_1X_2X_3$.

3. Results and discussion

The main results of our piezooptic studies are gathered in Table 3. The errors for the non-principal piezooptic coefficients are high enough. The lowest relative errors, 17% and 18%, are peculiar for the coefficients π_{64} and π_{52}. The coefficient π_{46} has been determined with the relative error exceeding 100%. The other coefficients have been measured with the errors 29–68%. Besides, the combination of coefficients $\pi_{51} + \pi_{53}$ has been derived with the error amounting to 94%. It is noteworthy that the method of measurements used by us does not enable determining these tensor components separately.

Table 3. Non-principal piezooptic coefficients for the TGS crystals determined at T = 293 K (1 Br = 10^{-12} m^2/N).

Experimental conditions			σ^o_{im}, kg/cm	π_{im}, Br
m	*k*	*i*		
Sample of *X*/45°-cut (Fig. 1b)				
$4(\bar{4})$	$\bar{4}(4)$	$4(\bar{4})$	$\sigma^o_{44} = \sigma^o_{\bar{4}\bar{4}} = 34.0$	$\pi_{44} = -3.7 \pm 2.2$
Sample of *Z*/45°-cut (Fig. 1d)				
$6(\bar{6})$	$\bar{6}(6)$	$6(\bar{6})$	$\sigma^o_{66} = \sigma^o_{\bar{6}\bar{6}} = 25.5$	$\pi_{66} = 3.2 \pm 2.2$
Sample of *Y*/45°-cut (Fig. 1c)				
2	5	$\bar{5}$	$\sigma^o_{\bar{5}2} = 20.2$	$\pi_{52} = 3.4 \pm 0.6$
5	2	1	$\sigma^o_{15} = 14.0$	$\pi_{15} = -6.3 \pm 1.8$
		3	$\sigma^o_{35} = 12.5$	$\pi_{35} = -2.8 \pm 1.7$
5	$\bar{5}$	5	$\sigma^o_{55} = 31.0$	$\pi_{55} = 5.7 \pm 2.2$
		2	$\sigma^o_{25} = 59.0$	$\pi_{25} = -1.6 \pm 0.6$
		1	$\sigma^o_{\bar{1}5} = 12.5$	$\pi_{15} = -6.3 \pm 1.8$

$\bar{5}$	2	3	$\sigma^{o}_{3\bar{5}} = 17.0$	$\pi_{35} = -2.8\pm1.7$
$\bar{5}$	5	$\bar{5}$	$\sigma^{o}_{\bar{5}\bar{5}} = 20.0$	$\pi_{51} + \pi_{53} = 1.7\pm1.6$
		2	$\sigma^{o}_{\bar{2}5} = 40.0$	$\pi_{25} = -1.6\pm0.6$
Sample of B, $\bar{4}$-cuts (Fig. 1e) and sample of B and $\bar{6}$-cuts (Fig. 1f)				
$\perp B$	$\bar{4}$	4	$\sigma^{o}_{4B} = 23.1$	$\pi_{46} = 0.5\pm2.1$
$\perp \bar{B}$	$\bar{4}$	4	$\sigma^{o}_{\bar{4}B} = 16.9$	
$\perp B$	$\bar{6}$	6	$\sigma^{o}_{6B} = 9.2$	$\pi_{64} = 17.1\pm3.0$
$\perp \bar{B}$	$\bar{6}$	6	$\sigma^{o}_{\bar{6}B} = 29.5$	

We have used another technique, a method of optical extinction of anisotropic sample between crossed polarizers. The direct-cut sample (see Fig. 1a) has been placed between the crossed linear polarizers so that the light propagates along the Y axis (k = 2) and the uniaxial load σ_m is applied along the X (m = 1) or Z (m = 3) axes. Under such conditions, the optical indicatrix rotates around the Y axis by a certain angle φ, which depends on the coefficients π_{51} or π_{53}:

$$\tan\varphi = \frac{\pi_{5m}\sigma_m}{B_1 - B_3}, \qquad (6)$$

We have $\varphi = (0.4\pm0.1)°$ under the conditions m = 3 and σ_3 = 300 kg/cm^2 and $\varphi \sqcup 0$ when m = 1 and σ_1 = 300 kg/cm^2. The magnitude of the π_{53} coefficient is equal to $|3.0 \pm 0.3|$ Br. Taking into account that the combined coefficient $\pi_{51} + \pi_{53}$ is equal to 1.7±1.6, one can find that the π_{53} coefficient is positive and π_{51} negative ($\pi_{51} = -1.3 \pm 1.6$). In other words, the above sum is almost zero, agreeing well with a zero angle of optical indicatrix rotation observed when the load is applied along the X axis. Accounting for the results of our work [31], we state that all of the piezooptic coefficients for the TGS crystals are now determined (see Table 3).

Table 3. Piezooptic coefficients for the TGS crystals (in Br).

π_{11}	π_{22}	π_{33}	$^*\pi_{12}$	$^*\pi_{21}$	π_{13}	π_{31}	π_{23}	π_{32}	π_{44}
–0.73 ±0.06	5.40 ±0.55	6.5 ±1.5	–1.1 ±1.9	0.7 ±1.0	8.2±2.7	–0.14 ±0.01	4.9 ±1.4	0.46 ±0.06	–3.7 ±2.2
π_{55}	π_{66}	$^*\pi_{46}$	π_{64}	$^*\pi_{51}$	π_{52}	π_{53}	π_{15}	π_{25}	π_{35}
5.7 ±2.2	3.2 ± 2.2	0.5 ±2.1	17.1 ±3.0	1.3 ±1.6	3.4 ±0.6	3.0 ±0.3	–6.3 ±1.8	–1.6 ±0.6	–2.8 ±1.7

As seen from Table 3, the four coefficients marked by asterisk, π_{12}, π_{21}, π_{46} and π_{51}, are determined with the relative errors that exceed 100%. However, the coefficient π_{51} can be accepted as being almost equal to zero, as we have already mentioned. In addition, we have checked out the values of the principal piezooptic coefficients obtained in the work [31]. It has been found that they agree well with the present results. The elastooptic coefficients calculated using Eqs. (1) are collected in Table 4. The errors for the

elastooptic parameters are calculated using the relations $\delta(\pi_{im}C_{mn}) = [(\delta\pi_{im}C_{mn})^2 + (\pi_{im}\delta C_{mn})^2]^{1/2}$. Note that the errors of determination of the elastooptic coefficients are, in general, high enough. They do not exceed 25% for nearly the half of the coefficients. Still higher errors (~ 60%) are peculiar for the coefficients p_{12} and p_{44}, while the relative errors for the coefficients p_{66}, p_{46} and p_{51} marked by asterisks in Table 4 exceed 100%. One can see from Table 4 that the largest elastooptic coefficients are those described by the tensor components p_{22}, p_{23} and p_{21}. These are the components that provide coupling with the electric field of diffracted optical wave parallel to the two-fold symmetry axis, i.e. the polar axis.

Table 4. Elastooptic coefficients calculated for the TGS crystals.

p_{11}	p_{22}	p_{33}	p_{12}	p_{21}	p_{13}	p_{31}	p_{23}	p_{32}	p_{44}
0.128 ±0.064	0.288 ±0.039	0.183± 0.039	0.125 ±0.083	0.227 ±0.055	0.196 ±0.080	0.139 ±0.031	0.256 ±0.043	0.149 ±0.032	–0.035 ±0.021
p_{55}	$^*p_{66}$	$^*p_{46}$	p_{64}	$^*p_{51}$	p_{52}	p_{53}	p_{15}	p_{25}	p_{35}
0.054 ±0.026	0.012 ±0.014	0.005 ±0.013	0.161 ±0.030	0.042 ±0.075	0.146 ±0.034	0.097 ±0.036	–0.102 ±0.024	–0.043 ±0.009	–0.058 ±0.020

Now we are in a position to consider the acoustooptic interactions that involve the elastooptic components mentioned above. Then the acoustooptic effect implies the coupling of the electric field E_2 of diffracted optical wave with the induction of the incident optical wave D_2 ($E_2 = \Delta B_{22} D_2$). In case of isotropic interaction with the quasi-longitudinal waves propagating along the *X*, *Y* and *Z* axes, we have $E_2 = p_{21} e_1 D_2$, $E_2 = p_{22} e_2 D_2$ and $E_2 = p_{23} e_3 D_2$, with e_n being the strain tensor component caused by the acoustic wave. Schematic vector diagrams corresponding to the Bragg acoustooptic interactions in the principal planes of optical indicatrix ellipsoid are presented in Fig. 2. Here the coefficients p_{22}, p_{23} and p_{21} play a role of effective elastooptic coefficients.

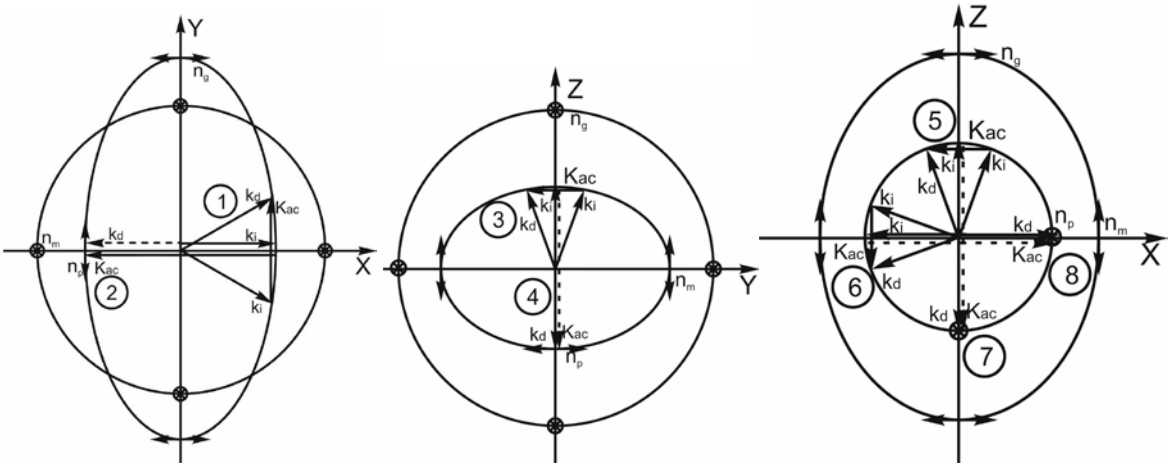

(a) (b) (c)

Fig. 2. Schematic vector diagrams of isotropic acoustooptic Bragg diffractions occurring in the principal planes *XY* (a), *YZ* (b) and *XZ* (c) in TGS. Labels 1, 3, 5 and 6 correspond to tangential Bragg diffractions, whereas 2, 4, 7 and 8 to collinear diffractions of a reflection type.

Now let us estimate the acoustooptic figure of merit defined as $M_2 = n_i^6 p_{ef}^2 / \rho v_{kl}^2$, where ρ = 1680 kg/m^3 [33] denotes the crystal density, p_{ef} the effective elastooptic coefficient and v_{kl} the acoustic wave velocity. Here the indices *k* and *l* correspond to the directions of propagation and polarization of the acoustic wave, respectively. We analyze the acoustooptic diffractions of eight different types schematically defined in Fig. 2. Solving the Christoffel equation (see Ref. [30]) and using the elastic-stiffness coefficients written in the *XYZ* coordinate system (see Table 2), one can determine the velocities of the quasi-longitudinal waves as $v_{11} = 5251$ m/s, $v_{22} = 4371$ m/s and $v_{33} = 3969$ m/s. The acoustooptic figures of merit for different types of the isotropic acoustooptic diffractions are collected in Table 5. Notice that the equality $n_i = n_p$ holds true for all of these cases.

Table 5. Effective elastooptic coefficients, acoustic wave velocities and acoustooptic figures of merit for TGS calculated for the case of acoustooptic diffraction occurring in the principal planes of optical indicatrix.

Type of diffraction (see Fig. 2)	1	2	3	4	5	6	7	8
p_{ef}	p_{22}	p_{21}	p_{22}	p_{23}	p_{21}	p_{23}	p_{21}	p_{23}
v_{ij}	v_{22}	v_{11}	v_{22}	v_{33}	v_{11}	v_{33}	v_{11}	v_{33}
M_2, 10^{-15} s^3/kg	6.4	2.3	6.4	6.8	2.3	6.8	2.3	6.8

It is worth noticing that the highest M_2 coefficients correspond to the interactions with relatively slow acoustic waves v_{33} and v_{22}. These coefficients are comparable with those obtained in our recent work [31] (5.9×10^{-15} s^3/kg). In particular, we have $p_{ef} = p_{31}$ in the latter case. Here we remark that a detailed analysis of M_2 anisotropy is not the aim of the present work. It can be performed only after the elastooptic coefficient is derived, e.g. with the Dixon–Cohen method.

In order to further check our results, we have computed the elastooptic coefficients, using a quantum-mechanical approach implemented recently into a known CRYSTAL program [22, 36, 37]. A hybrid functional augmented by a correction to take into account weak dispersive interactions (B3LYPD3) has been used within the density-functional theory. We have considered a fully relaxed structure: a = 9.3845, b = 12.6108, c = 5.5317 Å, and the angle between the directions (101) and (100) being equal to β^* = 110.21° [33]. The best agreement between the experimental and computation data (p_{13} = 0.251, p_{21} = 0.247, p_{22} = 0.284, p_{13} = 0.313 and p_{23} = 0.233) has been observed when the material coefficients differ by 2–22% from the elastooptic components obtained experimentally.

4. Conclusions

In the present work we have determined all the components of piezooptic tensor for monoclinic crystals. This task has been implemented on a canonical example of TGS crystals. In order to decrease the experimental errors, we have derived so-called simplified relations. They enable determining the non-principal piezooptic coefficients due to taking so-called symmetric experimental conditions into account. The relative errors for the piezooptic coefficients π_{64} and π_{52} coefficients are about 17 and 18%. The other coefficients are meas-

ured with higher relative errors, 29–68%. Such relatively small coefficients as π_{46}, π_{51}, π_{12} and π_{21} reveal still higher errors which exceed 100%. Finally, we have found that the highest piezooptic coefficient is equal to π_{64} = (17.1±3.0) Br.

Basing on the piezooptic coefficients thus measured and the literature data available for the elastic-stiffness tensor components, we have calculated the elastooptic coefficients. The corresponding relative errors are high enough. In particular, although these errors do not exceed 25% for nearly half of the coefficients, they increase higher (~ 60%) in case of the coefficients p_{12} and p_{44}, and become still higher for the coefficients p_{66}, p_{46} and p_{51} (more than 100%).

The highest elastooptic parameters are those corresponding to the tensor components p_{22}, p_{23} and p_{21}. It is these components that provide acoustooptic coupling of the diffracted electric field parallel to the two-fold symmetry (or polar) axis. The acoustooptic figures of merit have been estimated for the case of isotropic acoustooptic interactions occurring in the principal planes of the coordinate system *XYZ*, in which the elastooptic coefficients mentioned above play a role of effective parameters. These figures amount to 2.3, 6.4 and 6.8×10^{-15} s^3/kg. The last two values correspond to the interactions with the slow acoustic waves propagating along the *Y* and *Z* axes, respectively.

It is obvious that the acoustooptic figures of merit obtained for TGS are lower than the appropriate values known for such canonical acoustooptic materials as, e.g., TeO_2 [38–40] or Hg_2Cl_2 [41]. Nonetheless, the M_2 coefficients of the TGS crystals, which are transparent in the deep ultraviolet range, are higher than those typical for fused silica or KDP crystals. We remind that the latter materials are often used for acoustooptic operation of ultraviolet optical radiation. Moreover, since TGS are low-symmetry crystals, they can reveal much more promising ‘indirect-cut’ experimental geometries of acoustooptic interactions. In principle, the latter geometries can be characterized by notably higher acoustooptic figures of merit, when compared to those obtained in the present work. To analyze comprehensive the spatial anisotropy of M_2, one has to derive the elastooptic coefficients with higher precision than that typical for this work. This problem can be solved, using the Dixon–Cohen method and accounting for the results of the present study and, in particular, the signs of the elastooptic tensor components obtained by us.

Acknowledgement

The authors acknowledge financial support of the present study from the Ministry of Education and Science of Ukraine (the Project #0117U000802), the State Fund for Fundamental Researches of Ukraine (the Project F73/101-2016) and the Belarusian Republican Foundation for Fundamental Researches (the Project F16K-022).

References

1. Brewster D, 1816. On the communication of the structure of doubly-refracting crystals to glass, murite of soda, flour spar, and other substances by mechanical compression and dilation. Phil. Trans. 106: 156–178.
2. Narasimhamurty T. S. Photoelastic and electrooptic properties of crystals. New York: Plenum Press (1981).

3. Grakh I I and Mozhanskaya A F, 1971. A type of mechanically anisotropic, optically sensitive material. Mekhanika Polimerov. 5: 835–839.
4. Weber Y-J, 1995. Determination of internal strain by optical measurements. Phys. Rev. B. 51: 12209–12215.
5. Slezinger I I, Alievskaya A N and Mironov Yu V, 1985. Piezooptic devices. Izmeritelnaya Tekhnika. 12: 17–19.
6. Billardon M and Badoz J, 1966. Birefringence modulator. C. R. Acad. Sci. Ser. B. 262: 1672–1675.
7. Kemp J C, 1969. Piezo-optical birefringence modulators: new use for a long-known effect. J. Opt. Soc. Amer. 59: 950–954.
8. Auld B A, Acoustic fields and waves in solids. Malabar, FL: Krieger Publishing Company (1990).
9. Xu J and Stroud R, Acousto-optic devices: principles, design, and applications. New York: Wiley (1992).
10. Balakshii V I, Parygin V N and Chirkov L E, Physical fundamentals of acoustooptics. Moscow: Radio i Sviaz' (1985).
11. O. Mys, M. Kostyrko, M. Smyk, O. Krupych and R. Vlokh, Anisotropy of acousto-optic figure of merit in optically isotropic media. Appl. Opt. 53 (2014) 4616–4627.
12. O. Mys, M. Kostyrko, M. Smyk, O. Krupych and R. Vlokh, Anisotropy of acoustooptic figure of merit for TeO_2 crystals. 1. Isotropic diffraction. Ukr. J. Phys. Opt. 15 (2014) 132–154.
13. O. Mys, M. Kostyrko, O. Krupych and R. Vlokh, Anisotropy of acoustooptic figure of merit for $LiNbO_3$ crystals: Isotropic diffraction. Appl. Opt. 54 (2015) 8176–8186.
14. Mys Oksana, Kostyrko Myroslav and Vlokh Rostyslav. Anisotropy of acousto-optic figure of merit for $LiNbO_3$ crystals: anisotropic diffraction. Appl. Opt. 55 2439–2450 2016.
15. Mys Oksana, Krupych Oleh and Vlokh Rostyslav. Anisotropy of an acousto-optic figure of merit for $NaBi(MoO_4)_2$ crystals. Appl. Opt. 55 7941–7955 2016.
16. Dixon R W and Cohen M G, 1966. A new technique for measuring magnitudes of photoelastic tensor and its application to lithium niobate. Appl. Phys. Lett. 8: 205–207.
17. Dixon R W, 1967. Photoelastic properties of selected materials and their relevance for applications to acoustic light modulators and scanners. J. Appl. Phys. 38: 5149–5152.
18. B. H. Mytsyk, A. S. Andrushchak and G. I. Gasktvich, Comprehensive of studies piezo-optical effect in langasite crystals. Ukr. J. Phys. 52 (2007) 798–807.
19. B. G. Mytsyk, A. S. Andrushchak, N. M. Demyanyshyn, Y. P. Kost', A. V. Kityk, P. Mandracci and W. Schranz. Piezo-optic coefficients of MgO-doped LiNbO3 crystals. Appl. Opt. 48 (2009) 1904–1911.
20. B. G. Mytsyk, A. S. Andrushchak and Y. P. Kost', Static photoelasticity of gallium phosphide crystals. Crystallogr. Rep. 57 (2012) 124–130.
21. B. G. Mytsyk, Ya. P. Kost', N. M. Demyanyshyn, A. S. Andrushchak and I. M. Solskii, Piezo-optic coefficients of $CaWO_4$ crystals. Crystallogr. Rep. 60 (2015) 130–137.

22. B. Mytsyk, A. Erba, N. Demyanyshyn and O. Sakharuk, Piezo-optic and elasto-optic effects in lead molibdate crystals. Opt. Mater. 62 (2016) 632–638.
23. B. Mytsyk, N. Demyanyshyn, I. Martynyuk-Lototska and R. Vlokh, Piezo-optic, photoelastic, and acousto-optic properties of SrB_4O_7 crystals. Appl. Opt. 50 (2011) 3889–3895.
24. Vasylkiv Yu, Kvasnyuk O, Krupych O, Mys O, Maksymuk O and Vlokh R, 2009. Reconstruction of 3D stress fields basing on piezooptic experiment. Ukr. J. Phys. Opt. 10: 22–37.
25. Kvasnyuk O., Vasylkiv Yu., Krupych O. and Vlokh R. Preferable geometrical parameters of samples for piezooptic experiments. Ukr. J. Phys. Opt. 15 195–206 (2014).
26. Skab I, Smaga I, Savaryn V, Vasylkiv Yu and Vlokh R, 2011. Torsion method for measuring piezo-optic coefficients. Cryst. Res. & Technol. 46: 23–36.
27. Vasylkiv Yu, Savaryn V, Smaga I, Skab I and Vlokh R, 2011. On determination of sign of the piezo-optic coefficients using torsion method. Appl. Opt. 50: 2512–2518.
28. Krupych Oleg, Savaryn Viktoriya and Vlokh Rostyslav, Precise determination of full matrix of piezo-optic coefficients with a four-point bending technique: the example of lithium niobate crystals. 2014 Appl. Opt. 53 (10) B1–B7.
29. M. E. Lines and A. M. Glass, Principles and application of ferroelectrics and related materials. Clarendon Press, Oxford, 1977.
30. Y. I. Sirotin and M. P. Shaskolskaya, Fundamentals of Crystal Physics (Mir, Moscow, 1982).
31. B. Mytsyk, V. Shut, N. Demyanyshyn, S. Mozzharov, A. Erba, B. Kalynyak, O. Mys and R. Vlokh, Piezooptic coefficients and acoustooptic efficiency of TGS crystals. Ukr. J. Phys. Opt. 18 (2017) 46–54.
32. B. Mytsyk, Methods for the studies of the piezo-optical effect in crystals and the analysis of experimental data. I. Methodology for the studies of piezo-optical effect. Ukr. J. Phys. Opt. 4 (2003) 1–26.
33. Wood E A and Holden A N, 1957. Monoclinic glycine sulphate: crystallographic data. Acta Cryst. 10: 145–146.
34. Konstantinova V P, Silvestrova I M and Aleksandrov K S, 1959. Obtaining of triglycine sulphate crystals and their physical properties. Kristallogr. 4: 69–73.
35. Romanyuk M O, Kostetskyi O M and Viblyi I F, 1976. Dispersion and temperature dependence of refractive indices of pure triglycine sulphate crystals. Ukr. Fiz. Zhurn. 21: 207–209.
36. A. Erba, R. Dovesi, Photoelasticity of crystals from theoretical simulations. Phys. Rev. B. 88 (2013) 045121/1–8.
37. A. Erba, M. T. Ruggiero, T. M. Korter and R. Dovesi, Piezo-optic tensor of crystals from quantum-mechanical calculations. J. Chem. Phys. 143 (2015) 144504/1–8.
38. T. Yano and A. Watanabe, Acousto-optic figure of merit of TeO_2 for circularly polarized light. J. Appl. Phys. 45 (1974) 1243–1245.
39. O. Mys, M. Kostyrko, O. Krupych and R. Vlokh, Anisotropy of acoustooptic figure of merit for TeO_2 crystals. 2. Anisotropic diffraction. Ukr. J. Phys. Opt. 16 (2015) 38-60.

40. O. Mys, M. Kostyrko, B. Zapeka, O. Krupych and R. Vlokh, Anisotropy of acoustooptic figure of merit for TeO_2 crystals. 2. Anisotropic diffraction: Errata. Ukr. J. Phys. Opt. 17 (2016) 148-166.
41. M. P. Shaskolskaya (ed.), Acoustic crystals, Reference Book, Nauka, Moskow, 1982.